World Scientific
www.worldscientific.com

JAPAN SOCIETY OF CIVIL ENGINEERS
COASTAL ENGINEERING COMMITTEE

Coastal Engineering Journal, Vol. 59, No. 1 (2017) 1750003 (32 pages)

DOI: 10.1142/S0578563417500036

Upstream Propagation of Surges and Bores: Free-Surface Observations

Xinqian Leng and Hubert Chanson*

The University of Queensland, School of Civil Engineering, Brisbane QLD 4072, Australia

**h.chanson@uq.edu.au*

Received 20 August 2015
Accepted 18 October 2016
Published 11 January 2017

In a free-surface flow, a sudden increase in water depth induces a positive surge, also called compression wave or bore. Herein a physical study was conducted in relatively large-size rectangular channel with a smooth bed. The upstream propagation of breaking and undular bores were investigated with a broad range of Froude numbers Fr_1 ranging from 1.1 to 2.3. Both instantaneous and ensemble-averaged free-surface measurements were performed nonintrusively. The observations showed the occurrence of undular bores for $1 < Fr_1 < 1.2$ to 1.3, breaking bores for $Fr_1 > 1.4$ to 1.5, and breaking bores with secondary waves for 1.2–1.3 $< Fr_1 <$ 1.4–1.5. The propagation of a breaking bore was associated with an upward free-surface curvature immediately before the roller toe for $Fr_1 < 2$, and an abrupt increase in free-surface elevation with the passage of the breaking roller. The propagation of undular bores was characterized by a smooth upward free-surface curvature, followed by a smooth first wave crest and a train of secondary quasi-periodic undulations. For all tidal bores, the passage of the bore front was always associated with large free-surface fluctuations, occurring slightly after the arrival of the front. During the generation process, the positive surge formed very rapidly and the surge celerity increased very rapidly, reaching maximum values excess of the fully-developed bore celerity. With increasing time, the surge decelerated and the bore propagated at an early constant celerity for $(x_{gate} - x)/x_{gate} > 10$.

Keywords: Positive surges; tidal bores; tsunami bores; rivers; estuaries; physical modeling; free-surface measurements; celerity.

*Corresponding author.

1. Introduction

In an open channel, canal, river or estuary, a sudden increase in flow depth induces a positive surge, also called compression wave or bore [Henderson, 1966; Bryson, 1969; Liggett, 1994]. In an estuary, the flood tidal wave may become a tidal bore during the early flood tide in a narrow funneled channel under large tidal ranges [Tricker, 1965; Chen *et al.*, 1990; Chanson, 2011a] (Fig. 1). A related geophysical application is the up-river propagation of tsunami [Shuto, 1985; Tanaka *et al.*, 2011]. During the 26 December 2004 and 10 March 2011 tsunami disasters, the rapid advances of the tsunami waters caused massive inland damage, when tsunami bores followed rivers and canals [Tanaka *et al.*, 2012; Tolkova *et al.*, 2015]. In each situation, after its onset, the bore may be analyzed as a hydraulic jump in translation [Rayleigh, 1908; Lighthill, 1978].

Following the milestone investigation of Bazin [1865], physical studies of positive surges and bores included the works of Favre [1935], Benet and Cunge [1971], Yeh and Mok [1990], Treske [1994], Hornung *et al.* [1995], Chanson [2005, 2010a, 2010b, 2011b], Koch and Chanson [2008, 2009], Docherty and Chanson [2012], Gualtieri and Chanson [2011, 2012], Khezri and Chanson [2012], and Leng and Chanson [2015a, 2015b]. Table 1 presents a comparative summary of detailed laboratory studies. Mathematical and numerical studies of tidal bores encompassed

(a)

Fig. 1. Photographs of tidal bores propagating up-river. (a) Undular bore in *Canal à la Mer*, Carentan at Port de Brévands, near Carentan (France) on 19 May 2015 — Bore propagation from right to left — The bore celerity was about 5.5 m/s. (b) Undular bore of the Sée River at Le Bateau near Avranches (France) on 18 May 2015 — Looking downstream at the incoming bore. (c) Breaking bore of the Sélune River in Bay of Mont Saint Michel (France) on 19 October 2008 — Bore propagation from right to left.

(b)

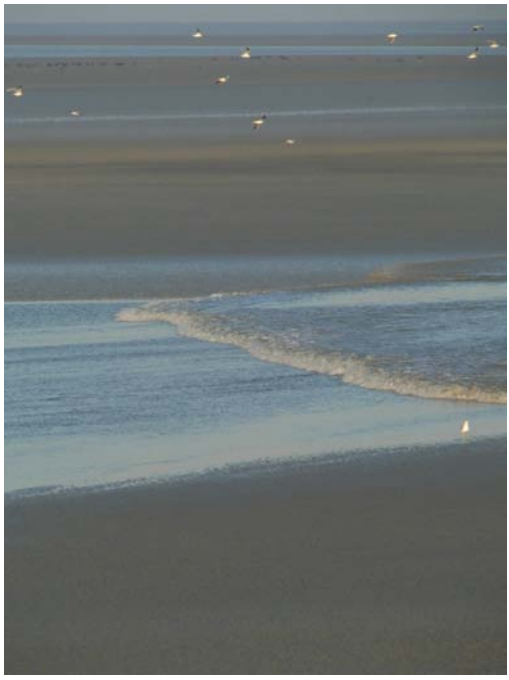

(c)

Fig. 1. (*Continued*)

depth-averaged models [Barré de Saint-Venant, 1871; Boussinesq, 1871, 1877; Peregrine, 1966; Madsen *et al.*, 2005; Pan *et al.*, 2007; Tolkova *et al.*, 2015], and more recently computational fluid dynamics (CFD) models [Furuyama and Chanson, 2010; Lubin *et al.*, 2010].

Table 1. Laboratory studies of positive surges and bores.

Reference	W (m)	S_o	Bed roughness	Q (m^3/s)	d_1 (m)	U (m/s)	Fr_1	Remarks
Present study	0.70	0	Smooth bed (PVC)	0.055–0.101	0.121–0.196	0.6–1.32	1.1–1.6	$L = 19$ m, $W = 0.7$ m.
		0.0025		0.071–0.101	0.113–0.143	0.46–0.92	1.2–1.6	
		0.005		0.055–0.101	0.072–0.105	0.25–0.77	1.6–2.1	
		0.0075		0.055–0.101	0.063–0.096	0.25–0.7	1.9–2.3	
Yeh and Mok [1990]	0.61	0	Smooth bed	0	0.04–0.06	—	1.35–2.07	$L = 16.5$ m, $W = 0.61$ m.
Hornung *et al.* [1995]	—	0	Smooth bed	0	—	—	1.5–6	$L = 24$ m.
Koch and Chanson [2009]	0.50	0	Smooth bed (PVC)	0.040	0.079	0.14–0.68	1.31–1.93	$L = 12$ m.
Chanson [2010b, 2011b]	0.50	0	Smooth bed (PVC)	0.058	0.137	0.56–0.90	1.17–1.49	$L = 12$ m, $W = 0.5$ m.
		0	Plastic screens	0.058	0.142	0.50–0.89	1.13–1.47	$k_s = 8$ mm, $L = 12$ m, $W = 0.5$ m.
		0.015–0.100	Smooth bed (PVC)	0.035–0.06	0.040–0.072	0.002–0.22	1.71–2.83	Decelerating bores, $L = 12$ m, $W = 0.5$ m.
Chanson and Tan [2010]	0.50	0	Smooth bed	0.013–0.058	0.050–0195	0.31–1.18	1.02–1.7	Neutrally buoyant particle tracking, $W = 0.5$ m.
Reichstetter [2011]	0.5	0	Smooth bed	0.020–0.030	0.064–0.086	—	1.1–1.4	$L = 12$ m, $W = 0.5$ m.
Gualtieri and Chanson [2011, 2012]	0.5	0	Smooth bed (PVC)	0.060	0.137–0.145	0.52–0.95	1.15–1.54	$L = 12$ m, $W = 0.5$ m.
Docherty and Chanson [2012]	0.5	0	Smooth bed (PVC)	0.050	0.117–0.119	0.29–0.85	1.08–1.65	$L = 12$ m, $W = 0.5$ m.
		0.002	Fixed gravel bed	0.050	0.125	0.31–0.88	1.01–1.52	$k_s = 3.4$ mm, $d_{50} = 5.7$ mm, $L = 12$ m, $W = 0.5$ m.
Khezri and Chanson [2012]	0.50		Fixed gravel bed	0.050	0.136	0.6–0.9	1.19–1.39	$k_s = 3.4$ mm, $d_{50} = 5.7$ mm, $L = 12$ m, $W = 0.5$ m.
			Mobile gravel bed	0.050	0.136	0.6–0.9	1.17–1.41	Live bed: $d_{50} = 5.7$ mm, $L = 12$ m, $W = 0.5$ m.
Simon and Chanson [2013]	0.50	0.0077	Fixed gravel bed	0.036 and 0.055	0.086–0.113	0.23–0.76	1.14–1.66	$k_s = 3.4$ mm, $d_{50} = 5.7$ mm, $L = 12$ m, $W = 0.5$ m.
Furgerot [2014]	0.50	0	Smooth bed (PVC)	0.017–0.072	0.097–0.187	0.79–1.12	1.26–1.58	$L = 16.5$ m, $W = 0.5$ m.
Chanson and Toi [2015]	0.50	0.0035	Smooth bed (PVC)	0.025	0.051	0.26–0.53	1.7–2.1	Physical modeling of a field data set, $L = 12$ m, $W = 0.5$ m.
Leng and Chanson [2015a]	0.70	0	Smooth bed (PVC)	0.085	0.146–0.165	0.90–0.99	1.33–1.49	$L = 19$ m, $W = 0.7$ m.

Notes: d_1: initial water depth; Fr_1: tidal bore Froude number; k_s: equivalent sand roughness height; L: test section length; Q: initial water discharge; S_o: bed slope; U: average bore celerity; W: channel width.

The shape of the surge is a function of its Froude number Fr_1 [Montes, 1998; Chanson, 2012]:

$$\mathrm{Fr}_1 = \frac{V_1 + U}{\sqrt{g \frac{A_1}{B_1}}}, \tag{1}$$

where V_1 is the initial velocity positive downstream, U is the surge celerity positive upstream, g is the gravity acceleration, A_1 is the initial flow cross-section area and B_1 is the initial free-surface width. An undular surge is typically observed for $\mathrm{Fr}_1 < 1.3$ to 1.5 [Figs. 1(a) and 1(b)], [Favre, 1935; Peregrine, 1966; Treske, 1994; Koch and Chanson, 2008; Chanson, 2010a]. For $\mathrm{Fr}_1 > 1.4$ to 1.6, the leading edge of the bore is characterized by a breaking roller [Fig. 1(c)] [Hornung *et al.*, 1995; Koch and Chanson, 2009; Khezri and Chanson, 2012]. The integral form of the equations of conservation of mass and momentum gives a series of relationships between the flow properties in front of and behind the bore front [Lighthill, 1978; Chanson, 2012]. For a sloping rectangular frictionless channel, the application of the continuity and momentum principle yields to a modified Bélanger equation:

$$\frac{d_2}{d_1} = \frac{1}{2} \times \left(\sqrt{(1-\varepsilon)^2 + 8 \times \frac{{\mathrm{Fr}_1}^2}{1-\varepsilon}} - (1-\varepsilon) \right), \tag{2}$$

where d is the flow depth, the subscripts 1 and 2 refer to the initial flow conditions and new conjugate flow conditions respectively, and ε is a dimensionless coefficient defined in terms of the bed slope $S_o = \sin\theta$ as:

$$\varepsilon = \frac{\text{Weight} \times S_o}{\rho \times g \times W \times {d_1}^2 \times ({\mathrm{Fr}_1}^2 - 1)} \tag{3}$$

with Weight being the weight force, W the channel width, ρ the water density, g the gravitational acceleration and θ the angle between the invert and horizontal [Leng and Chanson, 2015b]. For a horizontal frictionless rectangular channel, Eq. (2) yields the classical Bélanger equation:

$$\frac{d_2}{d_1} = \frac{1}{2} \times \left(\sqrt{1 + 8 \times {\mathrm{Fr}_1}^2} - 1 \right) \tag{4}$$

and, for a rectangular channel, the Froude number becomes: $\mathrm{Fr}_1 = V_1/(g \times d_1)^{1/2}$.

Herein a physical investigation was conducted with a focus on the generation and upstream propagation of bores. New experiments were conducted in a large facility. The observations included detailed free-surface measurements at a number of longitudinal locations for a broad range of flow conditions. For some flow conditions, experiments were repeated 25 times and the results were ensemble-averaged (EA). A comparative analysis between single measurements and EA data is developed, together with a re-analysis of both field and laboratory data. It is the aim of this work to characterize some seminal features of undular and breaking surges.

2. Experimental Setup and Surge Generation

2.1. *Presentation*

New experiments were conducted in a 19 m long 0.7 m wide rectangular flume with smooth PVC bed and 0.52 m high glass sidewalls. The initially steady flow was supplied by an upstream water tank leading to the 19 m long test section through a series of flow straighteners followed by a smooth bed and sidewall convergent. The water discharge was measured by a magneto flow meter with an accuracy of 10^{-5} m^3/s, carefully checked against brink depth data. A fast-closing Tainter gate was located next to the downstream end of the channel at $x = 18.1$ m, where x is measured from the upstream end of the flume. A radial gate was located further downstream at $x = 18.88$ m and was followed by a free overfall at $x = 19$ m.

Video observations were conducted using a HD video camera Sony^{TM} HDR-XR160, operating at 25 fps or 50 fps, with a resolution of 1920×1080 pixels, a digital camera Casio^{TM} Exlim EX-10, set at 120 fps (640×480 pixels), 240 fps (512×384 pixels) or 480 fps (224×160 pixels), and a dSLR camera Pentax^{TM} K-3 (movie resolution 1920×1080 pixels) equipped with Carl Zeiss^{TM} Distagon 28 mm f2 lens, producing photographs with a low degree (<1%) of barrel distortion. Photographic sequences in high-speed continuously shooting mode (8.3 fps) were also taken with the dSLR camera Pentax^{TM} K-3 (6016×4000 pixels). In steady flows, the water depths were measured using pointer gauges. The accuracy of the sharp pointer gauges was ± 0.5 mm. The unsteady water depths were recorded with a series of acoustic displacement meters (ADMs). A Microsonic^{TM} Mic+35/IU/TC unit was located at $x = 18.17$ m immediately downstream of the Tainter gate. Further nine ADMs Microsonic^{TM} Mic+25/IU/TC were spaced along the channel at $x = 17.81$, 17.41, 14.96, 12.46, 9.96, 8.5, 6.96, 3.96 and 0.96 m above the centerline. All ADMs were calibrated against the pointer gauge in steady flows and sampled at 200 Hz. Further details on the experimental facility and instrumentation were reported in Leng and Chanson [2015c].

2.2. *Experimental flow conditions and surge generation*

Four initially-steady discharges ($Q = 0.101$, 0.085, 0.071 and 0.055 m^3/s) were tested for the instantaneous free-surface measurements, with the highest and lowest discharges being used for the EA measurements. The tidal bore was generated by the rapid closure of the Tainter gate and the surge propagated upstream against the initially-steady flow. The Tainter gate closure time was less than 0.15–0.2 s, and such a closure time was small enough to have a negligible effect on the bore propagation. Appendix A presents some movies of the bore generation and propagation. For a given discharge, the bore Froude number was controlled by the gate opening h after closure, the initial flow depth d_1 and bed slope S_o. While the bulk of experiments were performed with a horizontal slope ($S_o = 0$), a steeper bed slope was used to generate larger bore Froude numbers (Appendix B). For the generation of undular

bores, the radial gate was initially closed partially to raise the initial water depth d_1. Figure 2(c) shows a schematic of the experimental facility with a partially-closed radial gate. The bores were generated by the rapid closure of the Tainter gate, with the radial gate position remaining unchanged during an experiment. For all breaking bore experiments, the radial gate was fully opened; the bore was generated by the rapid closure of the Tainter gate.

Both instantaneous and EA free-surface measurements were performed herein. For all experiments, the instruments were started 60 s before gate closure, and sampling stopped when the bore reached the upstream intake. During the EA

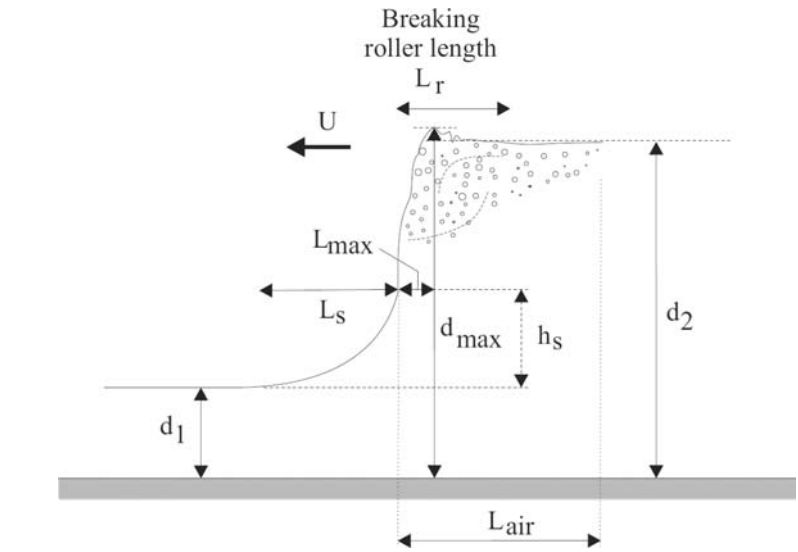

(a)

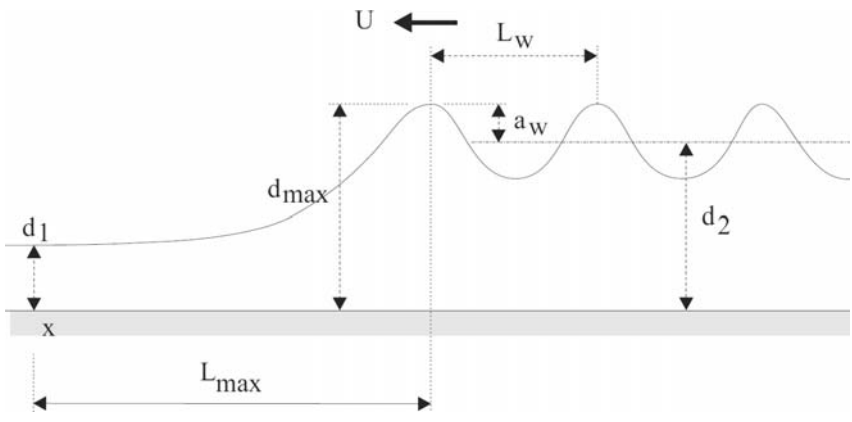

(b)

Fig. 2. Definition sketch of breaking and undular bores propagating upstream. (a) Sketch of a breaking bore front. (b) Sketch of an undular bore front. (c) Schematic of a tidal bore propagating upstream in the experimental facility.

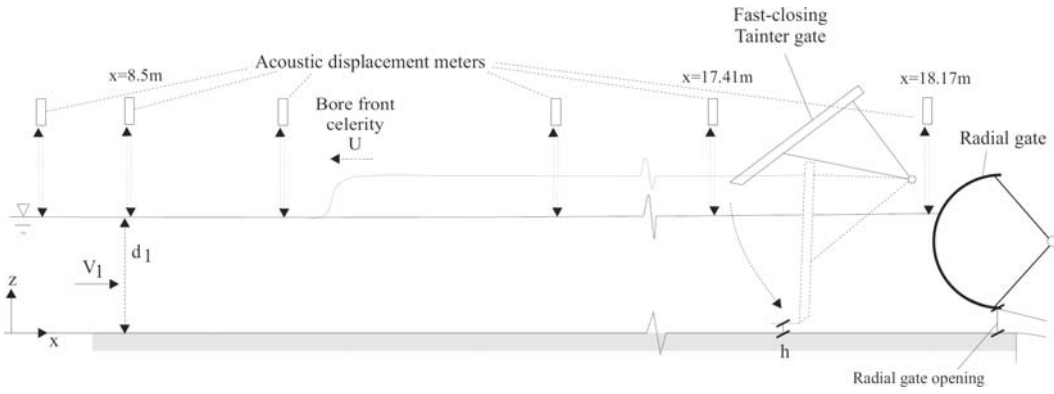

(c)

Fig. 2. (*Continued*)

experiments, a total of 25 runs were repeated for each set of controlled flow conditions; the median free-surface elevations and instantaneous free-surface fluctuations were calculated from the total ensemble. The experimental flow conditions are summarized in Table 1, where they are compared to past studies, and in Appendix B, together with the experimental observations at $x = 8.5$ m. Note that the present study was conducted a large facility with large flows (Table 1). Earlier dimensional analyses suggested that present results may be extrapolated to full-scale without adverse scale effects [Docherty and Chanson, 2012]. This will be confirmed in comparative presentations regrouping present results and prototype observations.

3. Flow Patterns

3.1. *Presentation*

Visual, video and photographic observations were conducted to document the basic flow patterns of the upstream propagation of tidal bores. Both breaking and undular bores were investigated. Figure 2 presents a definition sketch and Fig. 3 shows typical side views of the propagation of breaking and undular bores. For the present investigation, no bore was visible for a Froude number less than unity. For $1 < Fr_1 <$ 1.1 to 1.3, the bore was undular. The bore was characterized by a gentle upward free-surface rise and a series of quasi two-dimensional secondary undulations [Figs. 2(b) and 3(b) and movie CIMG0078.mov, Appendix A]. For $Fr_1 \geq 1.2$ there was no breaking, and small shock waves initiated from the sidewalls upstream of the first wave crest, intersecting at the first wave crest on the centerline [Fig. 3(c)].

Breaking bores with secondary waves developing behind the breaking roller were observed for 1.2 to 1.3 $< Fr_1 <$ 1.4 to 1.5. These bores were characterized by a thin layer of breaking developing at the bore front across most of the channel width, followed by a train of smooth, three-dimensional secondary waves. Herein

the expression "*breaking bore with secondary waves*" is used in line with Peregrine [1966]. Other researchers used the expression "*undular bore with some breaking*" to denote the same flow pattern [Koch and Chanson, 2009; Chanson, 2010b; Khezri and Chanson, 2012].

For $Fr_1 > 1.4$ to 1.5, the secondary wave motion disappeared and the breaking bore was characterized by a steep wall of water with a sharp breaking front [Figs. 2(a) and 3(a) and movie CIMG0007.mov, Appendix A). The propagation process was highly unsteady turbulent, with an abrupt rise in free-surface elevation and a rapidly fluctuating breaking roller [Leng and Chanson, 2015a]. The initially steady free-surface curved upwards slightly before the arrival of the breaking roller toe for Froude numbers smaller than 2, as illustrated in Figs. 2(a) and 3(a). Such an upward streamline curvature may be derived from theoretical considerations and was previously reported [Valiani, 1997; Chanson, 2010b; Docherty and Chanson, 2012]. For Froude numbers greater than 2, the upward streamline curvature was not

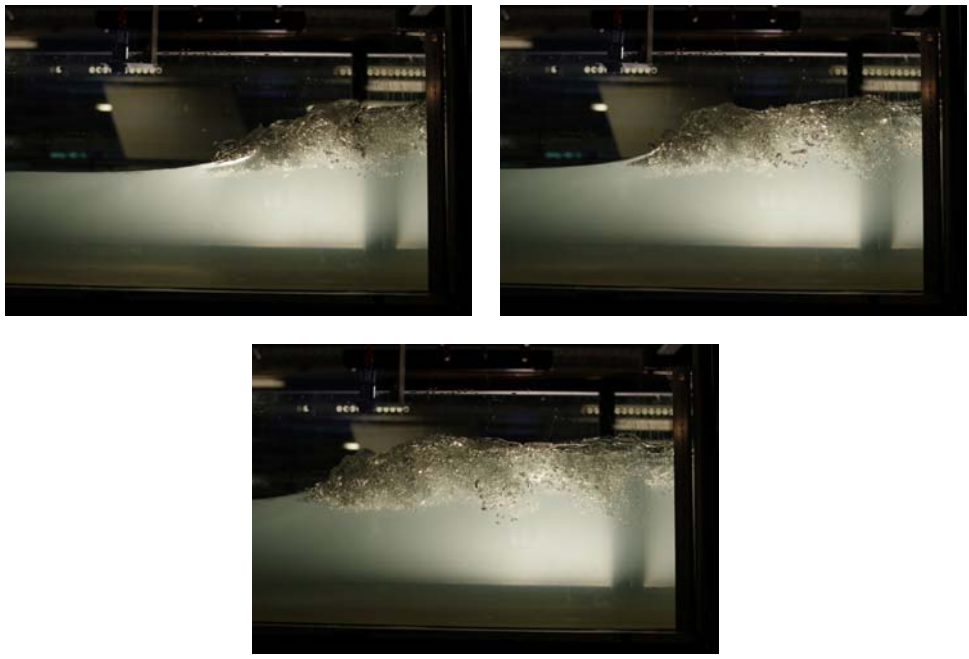

(a)

Fig. 3. Breaking and undular bore propagation. (a) Breaking bore propagation from right to left, viewed from the side with a time interval of 0.12 s between photographs; Flow conditions: $Q = 0.070\,m^3/s$, $S_o = 0$, Radial gate opening = fully-opened, $h = 0\,m$, $Fr_1 = 1.47$, high-shutter speed photographs (1/1, 600 s). (b) Undular bore propagation from right to left, viewed from the side with a time interval of 0.36 s between photographs; Flow conditions: $Q = 0.085\,m^3/s$, $S_o = 0$, Radial gate opening = 0.103 m, $h = 0.105\,m$, $Fr_1 = 1.1$, undular bore without sidewall shock waves, high-shutter speed photographs (1/320 s). (c) Undular bore with shock waves (arrows) at $x = 9.3\,m$ — Flow conditions: $Q = 0.101\,m^3/s$, $S_o = 0$, Radial gate opening = 0.125 m, $h = 0.071\,m$, $Fr_1 = 1.2$, Bore propagation from background to foreground.

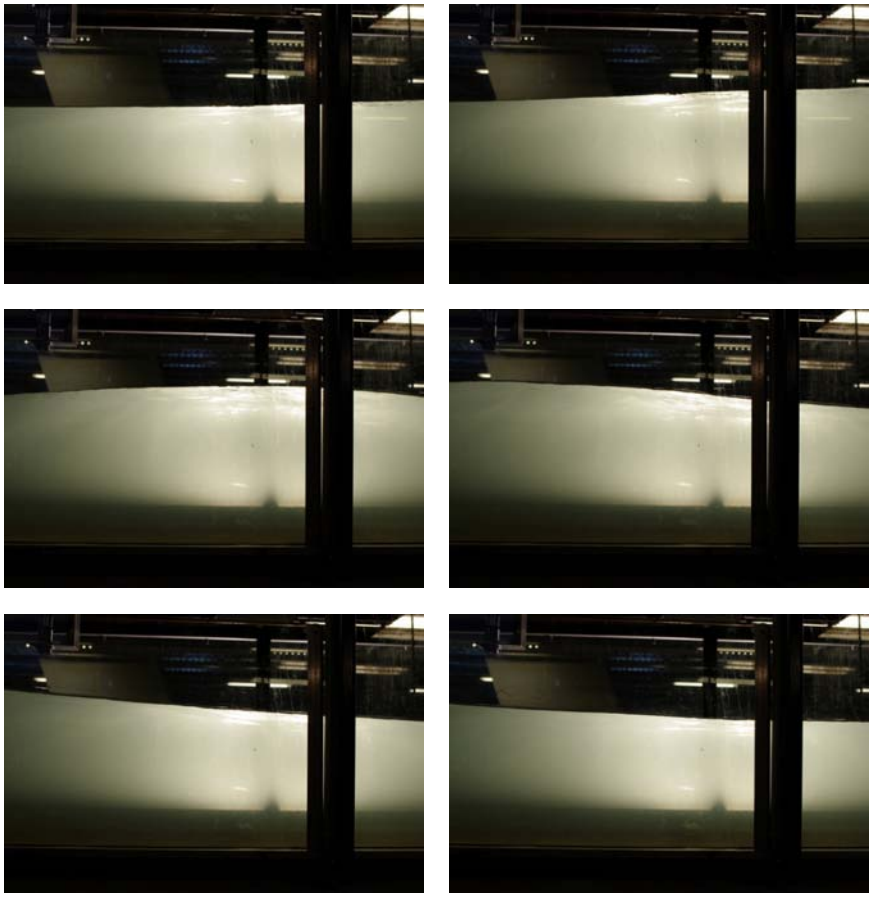

(b)

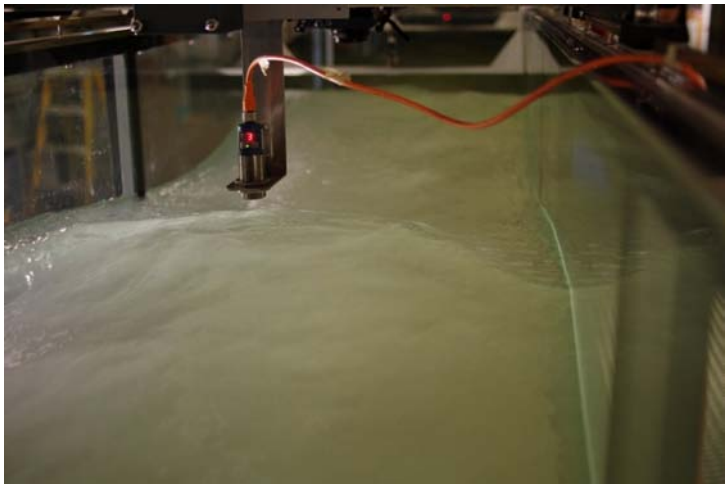

(c)

Fig. 3. (*Continued*)

seen. The breaking roller was characterized by a two-phase air–water flow region and strong turbulent interactions, with free-surface splashes and droplet ejection [Fig. 3(a)]. The free-surface was nearly horizontal behind the roller, although with large fluctuations.

The visual observations were consistent with earlier findings [Hornung *et al.*, 1995; Koch and Chanson, 2009; Chanson, 2010b; Chanson and Docherty, 2012; Khezri and Chanson, 2012].

3.2. *Instantaneous free-surface measurements*

Instantaneous free-surface measurements were recorded nonintrusively using the ADMs installed above the flume centerline. Figure 4 presents typical instantaneous free-surface measurements for two types of tidal bores: breaking [Fig. 4(a)] and undular [Fig. 4(b)]. In Fig. 4, t is the time since gate closure; and the thin red solid line is the ADM sensor located immediately downstream of the Tainter gate at $x = 18.17$ m. At that location, the sudden gate closure induced a negative surge associated with a drop in free-surface elevation. All other ADM sensors showed a marked rise in free-surface elevation associated with the passage of the bore, although some complicated transient flow pattern was observed immediately upstream of the gate ($x = 17.81$ m), as documented by Sun *et al.* [2016] in a smaller facility. The movies CIMG0006.mp4 and CIMG0080.mp4 show high-speed movies of the bore generation

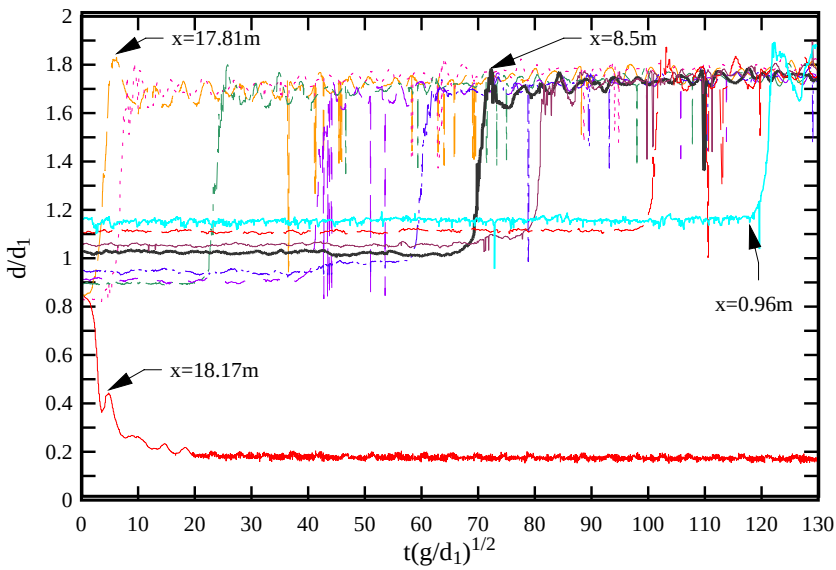

(a)

Fig. 4. Instantaneous free-surface variations as functions of time of breaking and undular bore with $t = 0$ at gate closure – Flow conditions: $Q = 0.101\,\mathrm{m}^3/\mathrm{s}$, $S_o = 0$. (a) Breaking bore — Radial gate opening = fully-opened, $h = 0$, $\mathrm{Fr}_1 = 1.6$. (b) Undular bore – Radial gate opening = 0.125 m, $h = 0.105$ m, $\mathrm{Fr}_1 = 1.1$.

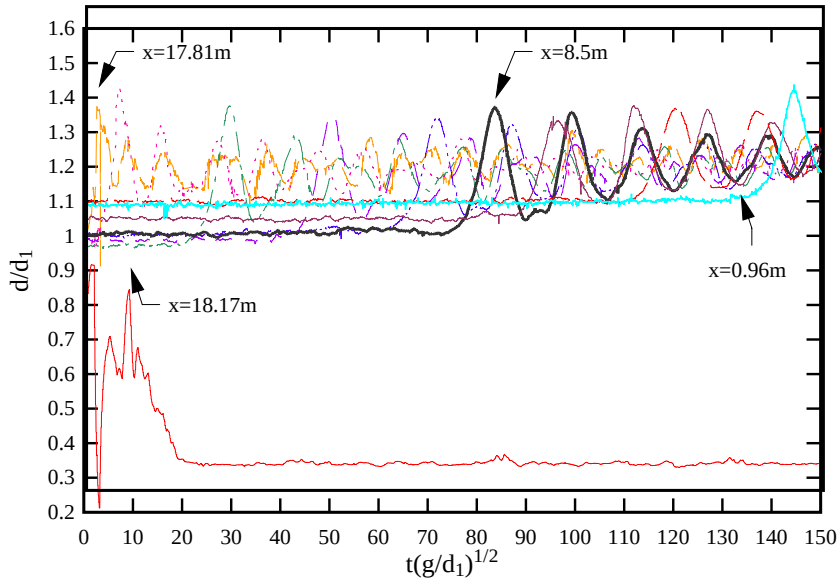

(b)

Fig. 4. (*Continued*)

induced by the Tainter gate closure (Appendix A). The propagation of the breaking bore was characterized by a sharp increase in water depths, followed by a fluctuating motion with nearly horizontal free-surface behind the marked roller [Fig. 4(a)]. The conjugate depth of the breaking bores was slightly lower than the peak elevation of the breaking roller and was highly fluctuating, as sketched in Fig. 2(a). The propagation of undular bores was associated with a smoother rise in water level, followed by a train of secondary undulations [Fig. 4(b)]. Overall the instantaneous ADM data were consistent with the photographic and video observations (Appendix A).

4. Free-Surface Properties

4.1. *Ensemble-averaged measurements*

The propagation of surges and bores is a highly turbulent and unsteady process, as illustrated by the high-speed movies (Appendix A). A time average would be meaningless and a series of EA measurements were conducted for two different discharges: that is, $Q = 0.101\ m^3/s$ and $0.055\ m^3/s$. Both breaking and undular bores were generated for each discharge. Further identical bore Froude number Fr_1 were achieved with different discharges (Appendix B). For each set of flow conditions, the experiments were repeated 25 times and the results were EA to obtain the median free-surface elevation d_{median} and the difference between the third and first quartiles ($d_{75} - d_{25}$). The difference between the third and first quartiles ($d_{75} - d_{25}$) characterized the instantaneous free-surface fluctuations. For a Gaussian distribution

of the data around its mean, $(d_{75} - d_{25})$ would be equal to 1.3 times the standard deviation of the total ensemble [Spiegel, 1972]. Figure 5 presents some typical EA data with the time variations of the free-surface elevation and fluctuations, where the time $t = 0$ corresponded to the Tainter gate closure. In each graph, the solid

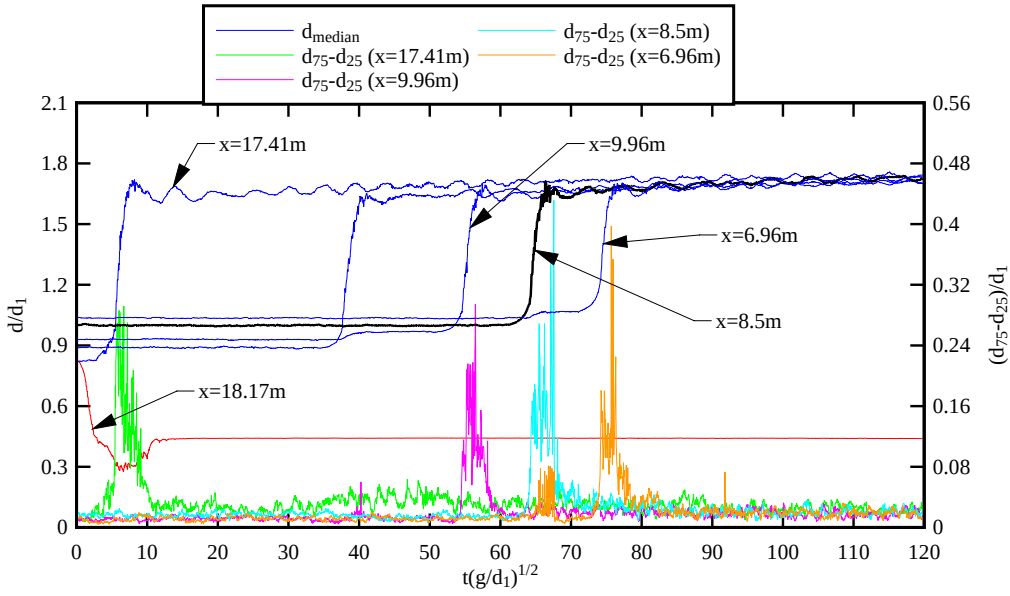

(a1)

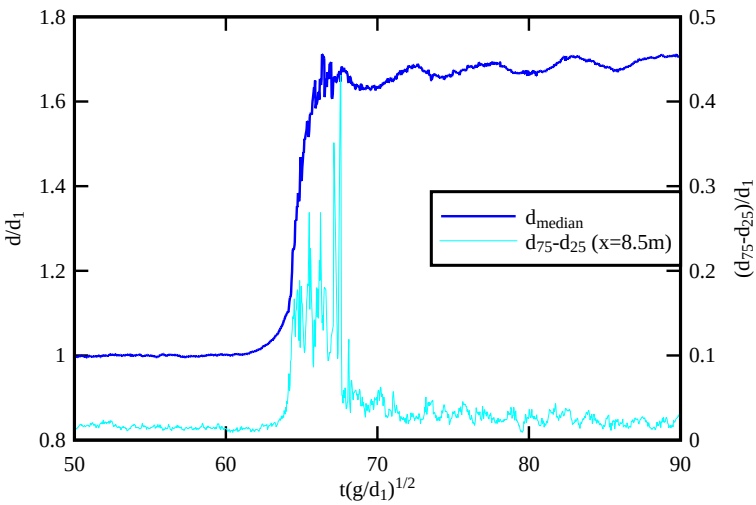

(a2)

Fig. 5. EA time variations of the median free-surface elevations and free-surface fluctuations at different longitudinal locations for breaking and undular bore (same legend for all graphs). (a) $Q = 0.101\,\mathrm{m}^3/\mathrm{s}$, $\mathrm{Fr}_1 = 1.5$, (a1) All data, (a2) Data at $x = 8.5\,\mathrm{m}$. (B) $Q = 0.101\,\mathrm{m}^3/\mathrm{s}$, $\mathrm{Fr}_1 = 1.2$, (b1) All data, (b2) Data at $x = 8.5\,\mathrm{m}$.

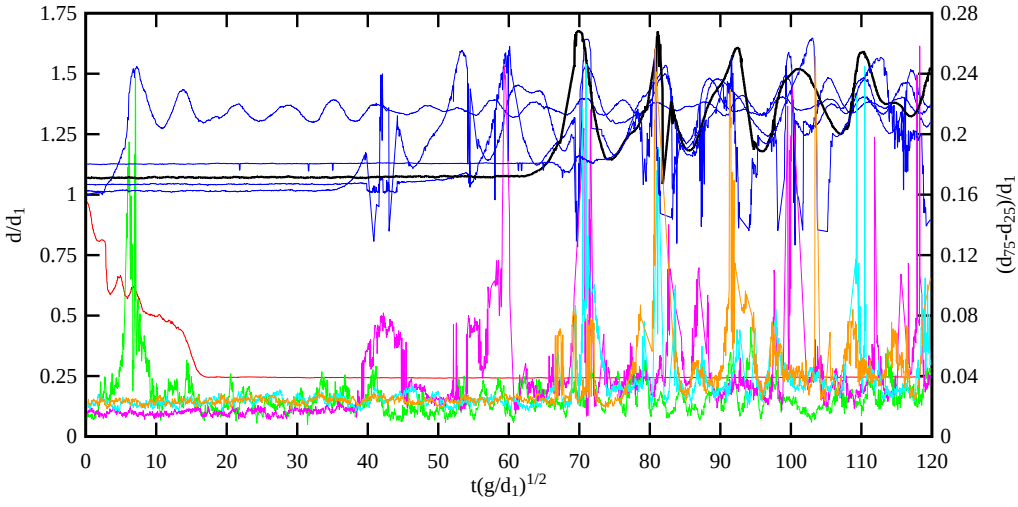

(b1)

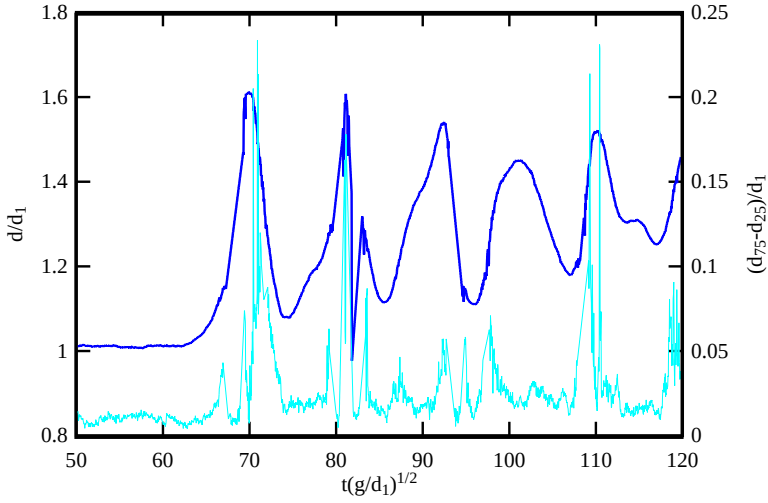

(b2)

Fig. 5. (*Continued*)

black line denotes the EA median free-surface elevation at $x = 8.5$ m, where the bore was fully-developed. Figure 5(a) shows breaking bore data, while Fig. 5(b) presents undular bore data.

For all breaking bore experiments, the EA free-surface data highlighted the abrupt increase in water level associated with the passage of the roller. After the roller, the free-surface increased very gradually. For the data at $x = 8.5$ m seen in Figs. 4(a) and 5(a), the dimensionless rate of increase in free-surface elevation was

on average $(\partial d/\partial t)/(g \times d_1)^{1/2} \sim 10^{-3}$ after the bore. The propagation of a breaking bore was typically associated with higher maximum free-surface fluctuations, than with undular bores, and these were caused by the highly turbulent breaking roller [Figs. 3(a) and 5], the free-surface fluctuations being quantified in terms of $(d_{75} - d_{25})$ herein. With breaking tidal bores, the free-surface fluctuations showed a marked maximum $(d_{75} - d_{25})_{\max}$ shortly after the passage of the bore breaking roller [Fig. 5(a)].

With undular bores, a key feature was the upward free-surface curvature ahead of the first wave crest, followed by a train of secondary undulations. The free-surface fluctuation data showed a sharp increase in free-surface fluctuations with the propagation of an undular tidal bore. A first local maximum free-surface fluctuation occurred shortly after the passage of the first wave crest, followed by a series of local maximum fluctuations appearing in a quasi-periodic manner during the secondary wave motion [Fig. 5(b)]. The time-variations of free-surface fluctuations in undular bores oscillated approximately in phase with the oscillations of the free-surface elevation.

The maximum free-surface fluctuation $(d_{75} - d_{25})_{\max}$ of breaking bores, the first maximum free-surface fluctuation $(d_{75} - d_{25})_{\max}$ of undular bores and the time lag Δt between the maximum fluctuation and bore front passage were analyzed for all flow conditions. Herein the time of the bore front passage was defined as the instant at which the free-surface elevation started to rise. Mathematically this corresponded to the time when the first derivative of the free-surface variation with respect to time was nonzero and positive. Figure 6 presents the experimental results as functions of longitudinal distance from the gate, where x_{gate} is the position of the Tainter gate. The data showed large maximum free-surface fluctuations relatively close to the gate: $(x_{\text{gate}} - x)/x_{\text{gate}} < 0.1$; further upstream large free-surface fluctuations were also observed over the entire channel length [Fig. 6(a)]. The time lag Δt increased rapidly with increasing distance from the gate and tended to reach a plateau $\Delta t/(g/d_1)^{0.5} \approx 5$ at about $(x_{\text{gate}} - x)/x_{\text{gate}} \approx 0.1$, before gradually increasing with increasing distance for $(x_{\text{gate}} - x)/x_{\text{gate}} > 0.4$ [Fig. 6(b)]. Importantly the largest maximum free-surface fluctuations were observed for the breaking bore with the highest Froude number ($\text{Fr}_1 = 2.2$) at almost all longitudinal locations. The dimensionless time lag was larger for the smallest water discharge ($Q = 0.055\,\text{m}^3/\text{s}$). Since the dimensionless results were presented assuming implicitly a Froude similitude, the finding might hint potential scale effects in terms of free-surface fluctuations.

4.2. *Bore propagation and celerity*

The position of the bore front and its celerity were deduced from the ADM data. Figure 7 presents typical data sets, with the bore front location and celerity presented as functions of the distance from the Tainter gate. Both single-run (Single) and EA data are shown. Overall the data showed the same distinctive trend for all Froude

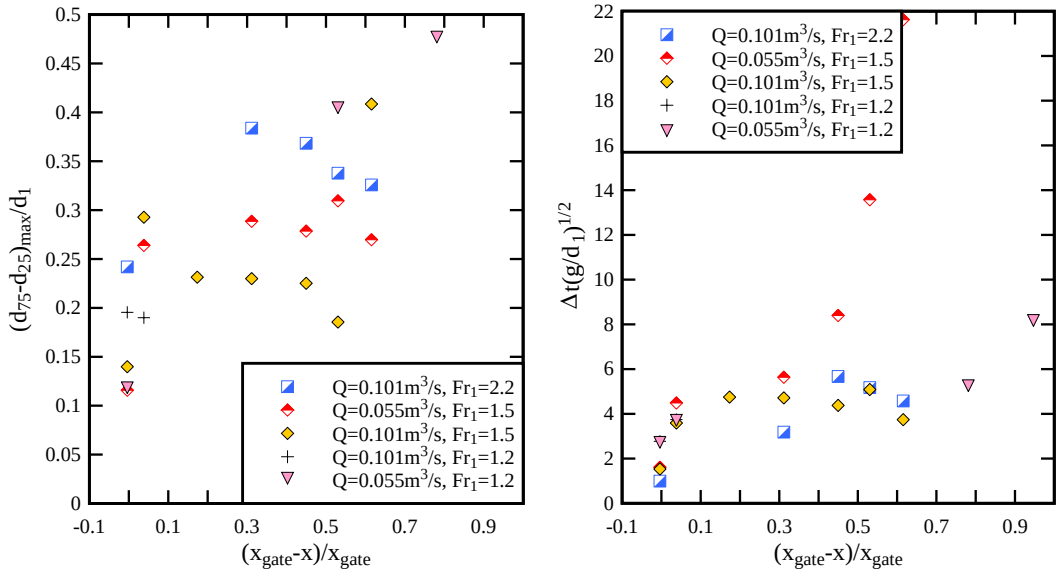

(a) (b)

Fig. 6. Maximum instantaneous free-surface fluctuations $(d_{75} - d_{25})_{\max}$ and time lag Δt between the maximum fluctuation and bore front passage as functions of the distance traveled by the bore. (a) Maximum instantaneous free-surface fluctuations $(d_{75} - d_{25})_{\max}$. (b) Time lag Δt between the maximum fluctuation and bore front passage.

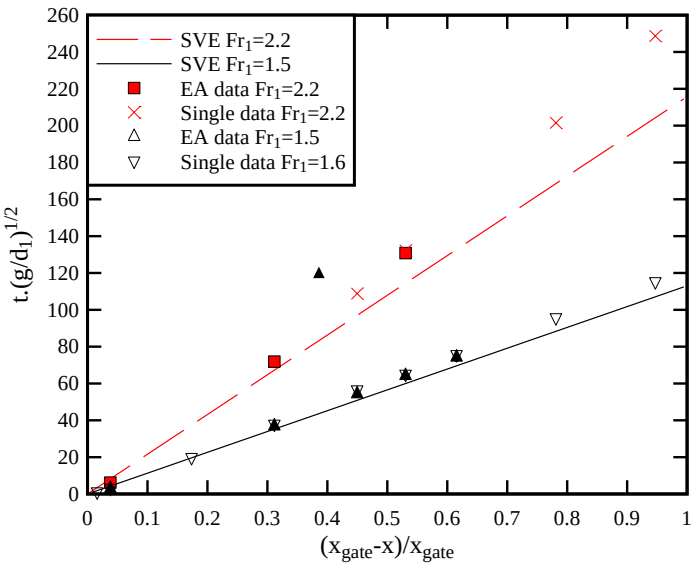

(a)

Fig. 7. Upstream propagation of breaking and undular bores — Comparison between single experiment (Single) and EA data. (a) Breaking bore front location as a function of the distance from the Tainter gate: comparison between experimental data and numerical solution of Saint-Venant equations (SVE) (solid line). (b) Bore front celerity as a function of the distance from the Tainter gate: breaking (Left) and undular (Right) bore data.

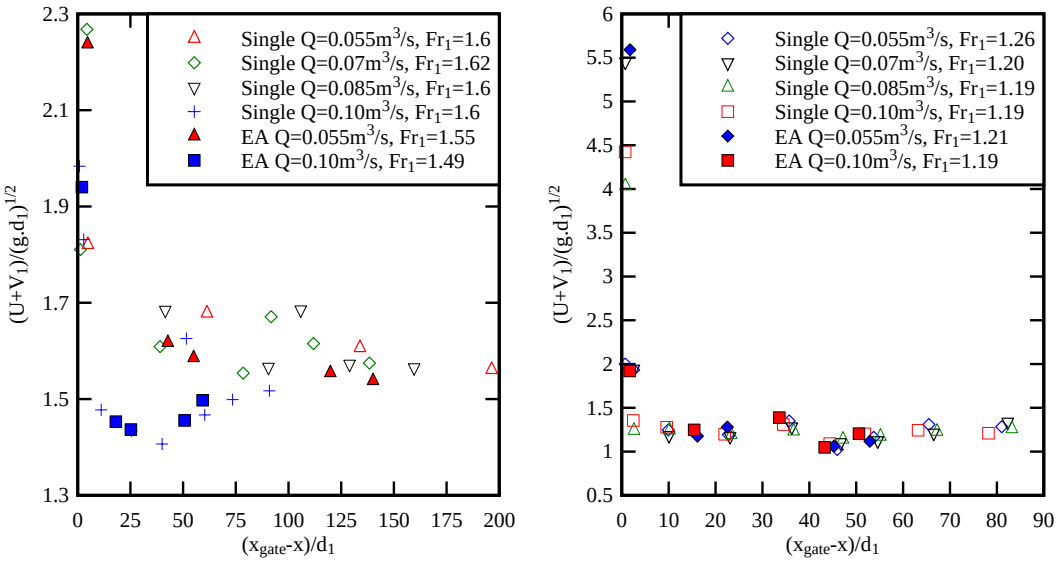

(b)

Fig. 7. (*Continued*)

numbers and flow rates. Immediately after the gate closure, the positive surge formed very rapidly and the process was associated with some strong disturbance immediately upstream of the gate (movies CIMG0006.MP4 and CIMG0080.MP4, Appendix A). The surge celerity increased very rapidly a very short distance, reaching maximum dimensionless value $(U + V_1)/(g \times d_1)^{1/2}$ well excess of the fully-developed bore properties observed for $(x_{\text{gate}} - x)/x_{\text{gate}} > 10$ [Fig. 7(b)]. For example, for $(x_{\text{gate}} - x)/x_{\text{gate}} < 10$, the dimensionless bore celerity reached values up to 2.3 for a breaking bore, and values in excess of 5 for undular bores. Further upstream, the surge decelerated and propagated in a more gradual manner, reaching its asymptotical value for $(x_{\text{gate}} - x)/x_{\text{gate}} > 10$. This asymptotical limit $(U + V_1)/(g \times d_1)^{1/2}$ was equal to the Froude number observed at $x = 8.5\,\text{m}$. The bore front location was relatively well predicted by the Saint-Venant equations as shown in Fig. 7(a). The present results differed from the observations of Reichstetter [2011], albeit her experiments were conducted for much smaller initially-steady discharges ($Q = 0.02$ and $0.03\,\text{m}^3/\text{s}$).

The dimensionless maximum water depth $(d_{\max} - d_1)/(d_2 - d_1)$ is shown in Fig. 8 as function of the dimensionless distance from the gate. For undular bores, the maximum wave height was that of the first wave crest. Basically the dimensionless maximum bore height was independent of the distance from the gate $(x_{\text{gate}} - x)/d_1 > 10$.

Altogether both visual observations and longitudinal measurements for a wide range of flow conditions indicated that the bore become fully-developed, that is a translating jump, for $(x_{\text{gate}} - x)/d_1 > 30$. Further upstream the free-surface properties varied little with upstream distance.

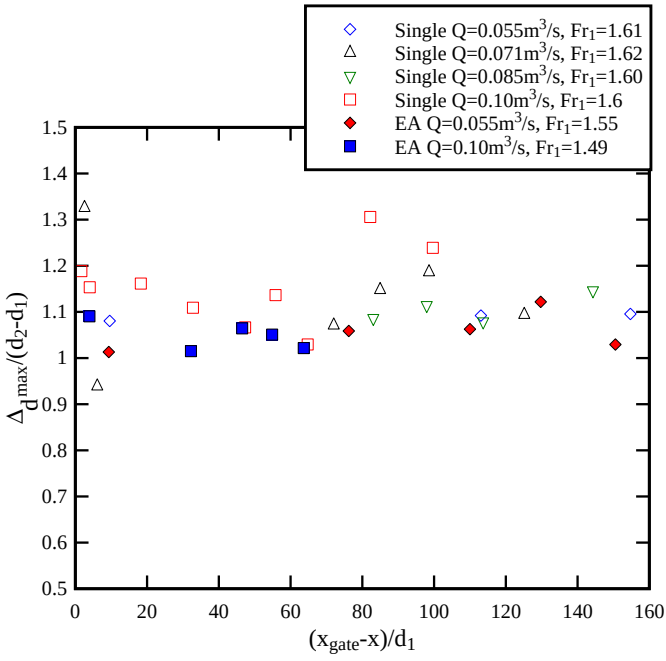

(a)

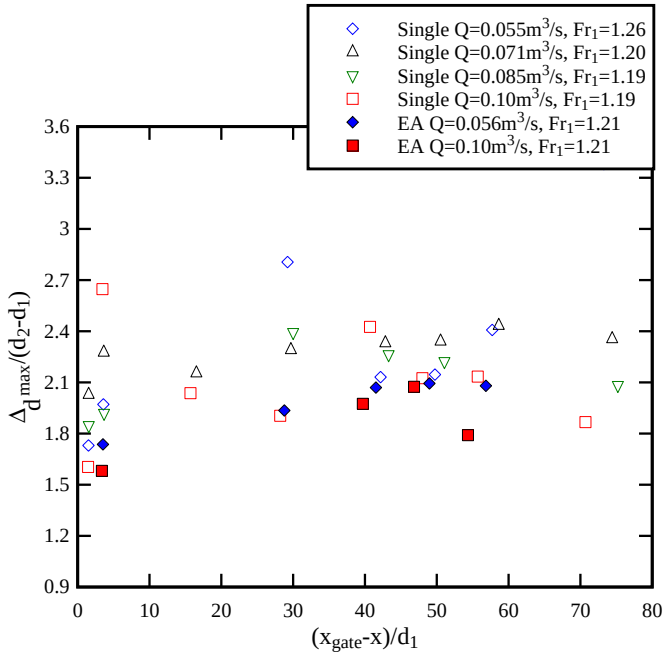

(b)

Fig. 8. Dimensionless maximum free-surface elevation $(d_{max}-d_1)/(d_2-d_1)$ as a function of distance from the Tainter gate — Comparison between single experiment (Single) and EA data. (a) Breaking bore. (b) Undular bore.

4.3. *Unsteady free-surface analysis*

The unsteady free-surface properties of fully-developed bores were analyzed based upon the free-surface measurements data at $x = 8.5$ m. The results were compared to theoretical developments and past experimental studies (field and laboratory). The key features of the bore front included the maximum water depth d_{max} and conjugate water depth d_2 for both breaking and undular bores (Fig. 2). For breaking bores, the roller length L_r, height and length of the rise in free-surface immediately upstream of the breaking roller toe h_s and L_s were specifically studied, as well as the distance L_{max} between the roller toe and the highest roller surface elevation. The wave amplitude a_w and wave length L_w were studied for undular bores. The definition sketch of these parameters is presented in Fig. 2. The full data are reported in tabular form in Appendix B.

The dimensionless conjugate water depth d_2/d_1 may be expressed as a function of the Froude number Fr_1, as shown in Eqs. (2) and (4) for a smooth sloping and horizontal rectangular channel, respectively. Equations (2) and (4) are compared to experimental observations in Fig. 9. All present data are presented with colored symbols, including both breaking and undular bores analyzed from video and ADM data (instantaneous and EA). All data showed a monotonic increase in conjugate depth ratio with increasing Froude number. The present data were compared to previous experimental works. Overall the experimental data with a horizontal bed slope showed a good fit with the Bélanger equation (Eq. (4)). For $1.6 < Fr_1 < 2.4$, the present data deviated from Eq. (4) because of the nonhorizontal bed setup; these data matched well with Eq. (2). The present data also compared well with previous experimental results (Fig. 9).

In a breaking bore with $Fr_1 < 2$, the free-surface ahead of the roller toe was curved upwards, as sketched in Fig. 2(a) and illustrated in Fig. 3(a), and discussed earlier. The longitudinal length and vertical height of this smooth curved surface are presented in Fig. 10 as functions of the Froude number Fr_1. The data include both instantaneous and EA measurements. The vertical height h_s of the roller toe above the initial water surface was best correlated by:

$$\frac{h_s}{d_1} = \frac{0.37}{Fr_1^{1.93}}, \quad 1.22 < Fr_1 < 2.3 \tag{5}$$

with a normalized correlation coefficient $R = 0.52$. Equation (5) is presented in Fig. 10(a), where it is compared with the present data as well as earlier experimental results. Altogether the observations indicated that both h_s and L_s decreased with increasing Froude number, tending asymptotically toward zero for $Fr_1 > 2.5$.

For breaking tidal bores, the length L_r of the roller was defined as the distance between the roller toe and the end of the breaking roller, where the water depth reached the conjugate depth d_2 [Fig. 2(a)]. The dimensionless roller length data are plotted as a function of the Froude number in Fig. 11. In Fig. 11, both instantaneous and EA measurements and the present data are compared with past studies of

Field observations	Laboratory data: Single observations	Laboratory data: EA observations
Benet and Cunge [1971], Lewis [1972]	Favre [1935], Benet and Cunge [1971], Koch and Chanson [2009], Chanson [2010a, 2010b], Docherty and Chanson [2012], Present study	Docherty and Chanson [2012], Khezri and Chanson [2012], Chanson and Toi [2015], Present study

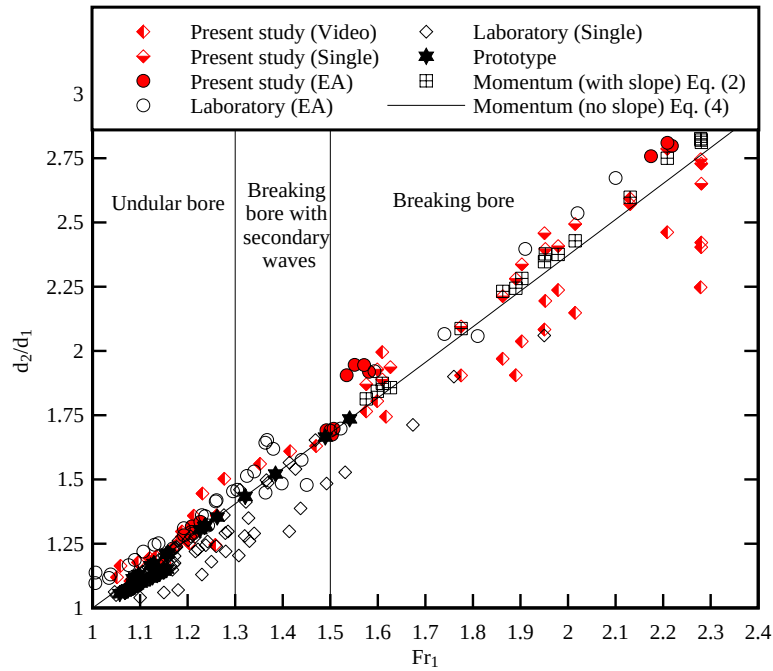

Fig. 9. (Color online) Dimensionless conjugate depth as a function of Froude number Fr_1 — Comparison between video (Video), single experiment (Single) and EA data — Present data in colored symbols include both video and ADM data for breaking and undular bores — Comparison with the momentum principle (Eqs. (2) and (4)) and earlier observations.

stationary hydraulic jumps. Figure 11 shows that, although the majority of Froude numbers tested herein were lower than those in stationary jump experiments, the present data with $Fr_1 > 2$ matched relatively closely stationary hydraulic jump data. Furthermore the present data trend showed a consistent decrease of roller length with decreasing Fr_1, in line stationary hydraulic jump data trend.

For an undular bore, two basic properties are the secondary wave amplitude and wave length, a_w and L_w, respectively [Fig. 2(b)]. Figure 12 shows both the dimensionless wave amplitude and wave length as functions of Froude number. The present data are compared to previous experimental data, a cnoidal wave solution [Andersen, 1978] and the linear wave theory of Lemoine [1948]. The former solution was

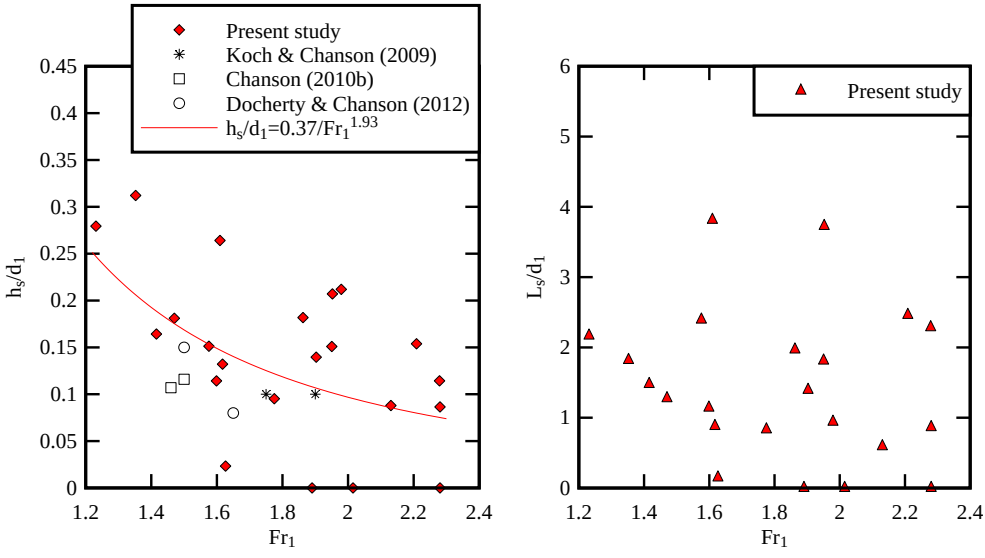

Fig. 10. Dimensionless height h_s/d_1 and length L_s/d_1 of upward curved free-surface in front of the breaking bore roller toe as functions of bore Froude number Fr_1 for breaking bores — Comparison with laboratory studies [Koch and Chanson, 2009; Chanson, 2010b; Docherty and Chanson, 2012]. (a) Height h_s of upward curved free-surface in front of the breaking bore roller toe — Comparison with Eq. (5). (b) Length L_s of upward curved free-surface in front of the breaking bore roller toe.

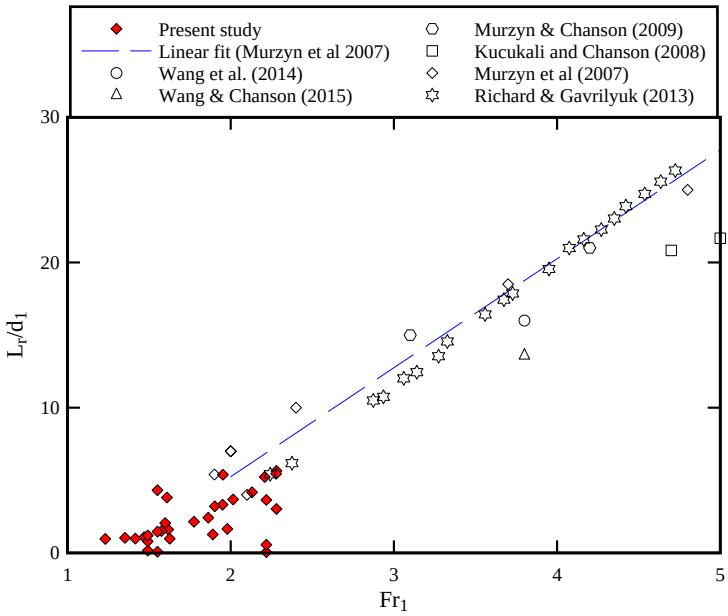

Fig. 11. Dimensionless roller length as a function of bore Froude number Fr_1 for breaking bores — Comparison with past studies of stationary hydraulic jumps [Kucukali and Chanson, 2008; Murzyn *et al.*, 2007; Murzyn and Chanson, 2009; Richard and Gavrilyuk, 2013; Wang *et al.*, 2014; Wang and Chanson, 2015].

based upon the Boussinesq equation and the asymptotical results for a rectangular channel are [Benjamin and Lighthill, 1954]:

$$\frac{a_w}{d_2} = \frac{1}{\sqrt{3}} \times \left(\frac{d_2}{d_1} - 1\right), \tag{6}$$

$$\frac{L_w}{d_2} = \frac{2 \times \pi \times \sqrt{2}}{\sqrt{3}} \times \left(\frac{d_2}{d_1} - 1\right)^{-1/2}. \tag{7}$$

The present data were analyzed in terms of both instantaneous and EA measurements. Altogether the results followed closely previous studies, with an increase in

Field observations	Laboratory data: Single observations	Laboratory data: EA observations
Benet and Cunge [1971], Lewis [1972], Wolanski *et al.* [2004], Chanson *et al.* [2011], Furgerot *et al.* [2013], Reungoat *et al.* [2014, 2015]	Favre [1935], Benet and Cunge [1971], Treske [1994], Koch and Chanson [2009], Chanson [2010a], Gualtieri and Chanson [2011], Docherty and Chanson [2012], Present study	Present study

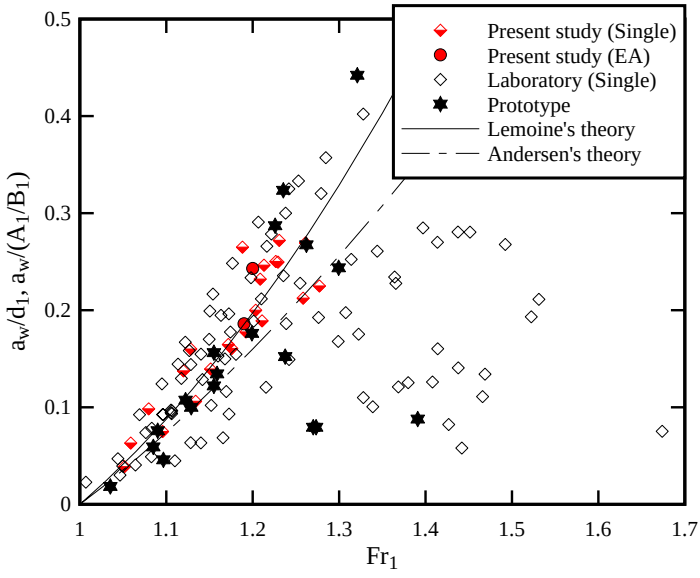

(a)

Fig. 12. Free-surface characteristics of undular bores — Present data in colored symbols. (a) Dimensionless wave amplitude as a function of Froude number Fr_1 for undular bores — Comparison with theory [Lemoine, 1948; Andersen, 1978], laboratory studies and field works. (b) Dimensionless wave length as a function of bore Froude number Fr_1 for undular bores — Comparison with theory [Boussinesq, 1871], laboratory studies and field work.

Field observations	Laboratory data: Single observations	Laboratory data: EA observations
Wolanski *et al.* [2004], Chanson *et al.* [2011], Furgerot *et al.* [2013], Reungoat *et al.* [2014, 2015]	Koch and Chanson [2009], Chanson [2010a], Gualtieri and Chanson [2011], Docherty and Chanson [2012], Present study	Khezri and Chanson [2012], Present study

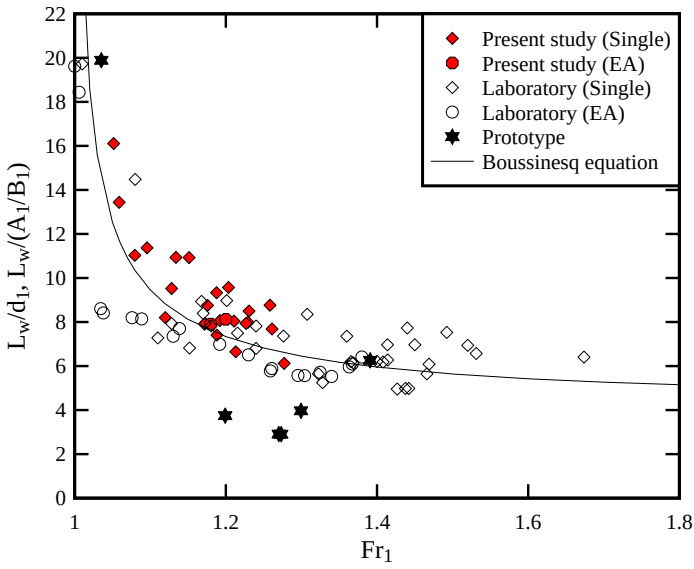

(b)

Fig. 12. (*Continued*)

wave amplitude and monotonic decrease in wave length with increasing Froude number for $Fr_1 < 1.3$. In Fig. 12, the field data are presented in dimensionless terms using the characteristic length scale A_1/B_1, as indeed the ratio of initial cross-sectional flow area to channel width A_1/B_1 is the equivalent water depth f or an irregular channel cross-section [Henderson, 1966; Chanson, 2012]. Detailed quantitative data in terms of free-surface characteristics are summarized in a tabular form in Appendix B.

4.4. *Discussion*: *Relationship between specific momentum and energy in undular flow*

A key feature of undular bores is the secondary wave motion [Figs. 2(b) and 3(b)]. In positive surge and hydraulic jumps, the equation of conservation of momentum may be applied across the jump front together with the equation of conservation of mass [Henderson, 1966; Liggett, 1994; Montes, 1998]. When the rate of energy

dissipation is negligible as in an undular bore, there is a quasi-conservation of energy. In the system of coordinates in translation with the undular surge, the equations of conservation of momentum and energy become:

$$\frac{M}{{d_c}^2} = \frac{d_c}{d} + \frac{1}{2} \times \left(\frac{d}{d_c}\right)^2 = \frac{d_c}{d_1} + \frac{1}{2} \times \left(\frac{d_1}{d_c}\right)^2, \tag{8}$$

$$\frac{E}{d_c} = \frac{d}{d_c} + \frac{1}{2} \times \left(\frac{d_c}{d}\right)^2 = \frac{d_1}{d_c} + \frac{1}{2} \times \left(\frac{d_c}{d_1}\right)^2, \tag{9}$$

where M is the momentum function, E is similar to the energy per unit mass, also called the specific energy, and d_c is the critical flow depth which is equals for a bore:

$$d_c = \sqrt[3]{\frac{((V_1 + U) \times d_1)^2}{g}}. \tag{10}$$

Equation (8) is always valid but Eq. (9) is an approximation only applicable to an undular bore with a Froude number close to unity in absence of energy loss. Equations (8) and (9) may be considered as a parametric representation of the relationship between the dimensionless momentum $M/{d_c}^2$ and energy E/d_c [Benjamin and Lighthill, 1954; Montes, 1986; Chanson, 2010a] The function M–E consists of two branches intersecting at $M/{d_c}^2 = 1.5$ and $E/d_c = 1.5$ (Fig. 13) and these branches represent the only possible relationship between $M/{d_c}^2$ and E/d_c as long

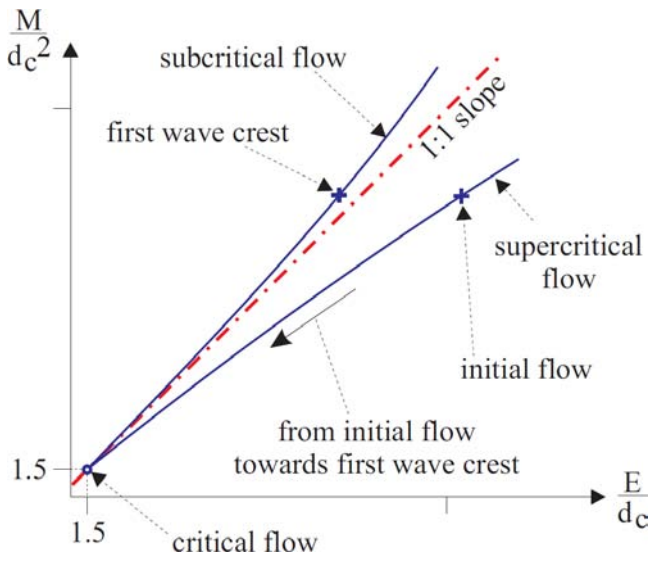

(a)

Fig. 13. Dimensionless relationship between specific momentum and energy in undular bores. (a) Sketch of the relationship between specific energy and momentum in undular flows. (b) Experimental data for $Q = 0.101\,\mathrm{m}^3/\mathrm{s}$, $B = 0.7\,\mathrm{m}$, $d_1 = 0.200\,\mathrm{m}$, $\mathrm{Fr}_1 = 1.19$, $U = 0.943\,\mathrm{m/s}$, $x = 8.5\,\mathrm{m}$, $S_o = 0$.

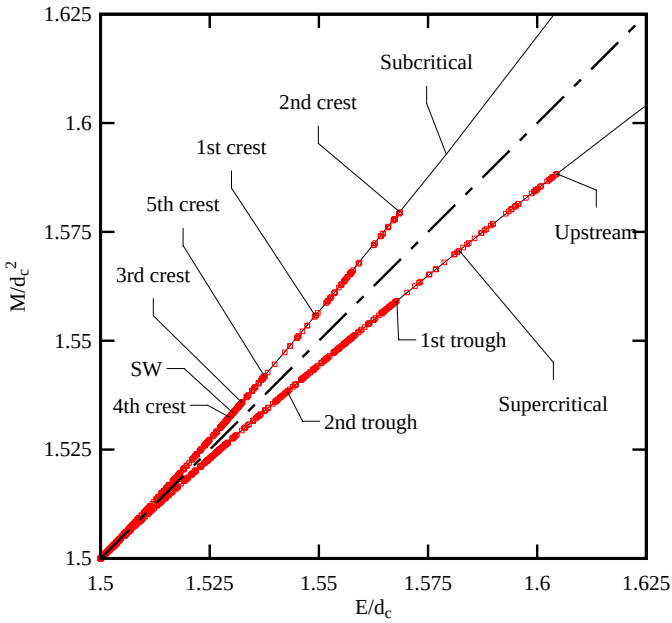

(b)

Fig. 13. (*Continued*)

as both the equations of conservation of momentum and energy (Eqs. (8) and (9)) hold. Figure 13(b) shows a comparison between Eqs. (8) and (9), and experimental data. The graph includes the initial flow conditions (label upstream) and the undular flow data up to the fifth wave crest. The onset of the shockwaves at sidewalls, upstream of the first wave crest, is shown (label SW). All data were located on the parametric diagram M–E. In Fig. 13(b), note all the wave crest data located on the left branch, with a smaller specific energy than that of the upstream flow (label upstream). This was because Eqs. (8) and (9) are based upon the assumption of hydrostatic pressure distribution; but the free-surface curvature at the first wave crest implies a pressure gradient less than hydrostatic, i.e. a smaller specific energy.

5. Conclusion

The free-surface properties were studied during the upstream propagation of positive surges and bores in a relatively large-size rectangular channel with a smooth bed. Both breaking and undular bores were investigated for a broad range of Froude numbers Fr_1 ranging from 1.1 to 2.3. The free-surface elevations were measured nonintrusively along the entire channel length. Both instantaneous and EA measurements were conducted. For some test conditions, the experiments were repeated 25 times and the data were EA. This approach provided a characterization of the instantaneous free-surface elevation median and fluctuations.

Visual, instantaneous and EA free-surface observations showed free-surface properties similar to those found in previous studies. Namely the occurrence of undular bores for $1 < Fr_1 < 1.2$ to 1.3, breaking bores for $Fr_1 > 1.4$ to 1.5, and breaking bores with secondary waves for $1.2–1.3 < Fr_1 < 1.4–1.5$. The propagation of a breaking bore was associated with an upward free-surface curvature immediately before the roller toe, and an abrupt increase in free-surface elevation with the passage of the breaking roller. The slope of the upward free-surface curvature decreased with increasing Froude number and disappeared for $Fr_1 > 2$. The propagation of undular bores was associated with a smooth upward free-surface curvature, followed by a smooth first wave crest and a train of secondary quasi-periodic undulations. For all tidal bores, the passage of the bore front was always associated with large free-surface fluctuations, characterized by the difference between the third and first quartiles ($d_{75} - d_{25}$). The data showed maximum free-surface fluctuation occurring slightly after the arrival of the front.

During the generation process, the positive surge formed very rapidly, with strong disturbance immediately upstream of the gate. The surge celerity increased very rapidly, reaching maximum values excess of the fully-developed bore celerity. With increasing time, the surge decelerated and continued to propagate upstream in a more gradual manner, reaching an asymptotical value for $(x_{gate} - x)/x_{gate} > 10$. The bore front location was relatively well predicted by the Saint-Venant equations. More the present data set indicated a close agreement between single-experiment and EA data, once the bore was fully-developed.

Lastly the present data were analyzed in terms of both single-run and EA data, because most literature to date used single-run data. However, the present study showed that the ensemble-averaging method is essential to high quality, while it provides further details in the instantaneous free-surface fluctuations.

Acknowledgments

The authors thank Professor Pierre Lubin (University of Bordeaux, France) for his advice, Dr Carlo Gualtieri (University of Napoli "Federico II", Italy), and Professor Shin-ichi Aoki (Osaka University, Japan) for their valuable comments. The authors acknowledge the technical assistance of Jason Van Der Gevel and Stewart Matthews (The University of Queensland). The financial support through the Australian Research Council (Grant DP120100481) is acknowledged.

Appendix A. High-Speed Movies of Tidal Bore Experiments

Visual observations of surges and bores were carried out for a wide range of flow conditions in a 19 m long 0.7 m wide rectangular flume with smooth PVC bed and 0.52 m high glass sidewalls. High-speed video movies were obtained using a digital camera Casio^{TM} Exlim Ex10 (120 fps, resolution: 640p × 480p; 240 fps, resolution:

512p × 384p, 480 fps, resolution: 224p × 160p). The movies are replayed at 30 fps: e.g. a 120 fps movie is hence replayed at 25% normal speed. In some movies, a metallic ruler is seen along the glass sidewall (e.g. movies CIMG0007.MOV and CIMG0078.MOV): the ruler was 334 mm high and 25 mm wide. The table below describes the video movies.

List of high-speed video movies, which can be viewed at http://www.worldscientific.com/worldscinet/cej, are:

Filename	Format	Description
CIMG0006.MP4	Resolution: 512 × 384 pixels Frame rate: 240 fps	Breaking bore generation induced by the rapid gate closure. Gate closure sequence. Flow conditions: $Q = 0.10\,m^3/s$, $d_1 = 0.172\,m$ at $x = 8.5\,m$, $S_o = 0$, $h = 0\,m$, $Fr_1 = 1.62$ at $x = 8.5\,m$, Radial gate: fully opened
CIMG0007.MOV	Resolution: 512 × 384 pixels Frame rate: 240 fps	Breaking bore propagation at $x = 8.5\,m$. Flow conditions: $Q = 0.101\,m^3/s$, $d_1 = 0.172\,m$ at $x = 8.5\,m$, $S_o = 0$, $h = 0\,m$, $Fr_1 = 1.62$ at $x = 8.5\,m$, Radial gate: fully opened
CIMG0080.MP4	Resolution: 224 × 160 pixels Frame rate: 480 fps	Undular bore generation induced by the rapid gate closure. Gate closure sequence. Flow conditions: $Q = 0.10\,m^3/s$, $d_1 = 0.200\,m$ at $x = 8.5\,m$, $S_o = 0$, $h = 0.071\,m$, $Fr_1 = 1.19$ at $x = 8.5\,m$, Radial gate opening: 0.125 m
CIMG0078.MOV	Resolution: 640 × 480 pixels Frame rate: 120 fps	Undular bore propagation at $x = 8.5\,m$. Flow conditions: $Q = 0.10\,m^3/s$, $d_1 = 0.200\,m$ at $x = 8.5\,m$, $S_o = 0$, $h = 0.071\,m$, $Fr_1 = 1.19$ at $x = 8.5\,m$, Radial gate opening: 0.125 m

Appendix B. Free-Surface Properties: Tabular Data Set

B.1. *Breaking tidal bore free-surface properties at $x = 8.5\,m$ (Present study)*

S_o	Q) (m^3/s	Radial gate opening (m)	h (m)	Fr_1	d_1 (m)	d_{max}/d_1	d_2/d_1	h_s/d_1	L_s/d_1	L_r/d_1
0	0.101	N/A	0	1.6	0.172	1.920	1.744	0.132	0.881	1.612
0	0.101	N/A	0.071	1.2	0.173	1.561	1.445	0.279	2.168	0.963
0	0.071	N/A	0	1.5	0.140	1.766	1.630	0.181	1.277	1.087

(*Continued*)

S_o	Q) (m^3/s	Radial gate opening (m)	h (m)	Fr_1	d_1 (m)	d_{max}/d_1	d_2/d_1	h_s/d_1	L_s/d_1	L_r/d_1
0	0.071	N/A	0.017	1.4	0.140	1.544	1.610	0.164	1.478	0.986
0	0.071	N/A	0.031	1.4	0.140	1.717	1.561	0.312	1.821	1.040
0.0025	0.101	N/A	0	1.6	0.143	0.853	0.830	0.023	0.149	0.979
0.005	0.101	N/A	0	2.1	0.105	2.330	2.593	0.088	0.593	4.176
0.005	0.101	N/A	0.071	1.8	0.105	2.167	1.905	0.095	0.833	2.143
0.005	0.085	N/A	0	2.0	0.098	2.308	2.237	0.212	0.942	1.648
0.005	0.085	N/A	0.071	1.6	0.098	1.828	1.805	0.114	1.142	2.056
0.005	0.071	N/A	0	2.0	0.085	1.964	2.148	0.000	0.000	3.683
0.005	0.071	N/A	0.071	1.6	0.085	1.891	1.765	0.151	2.395	1.513
0.005	0.055	N/A	0	2.0	0.072	2.114	2.083	0.151	1.812	3.321
0.005	0.055	N/A	0.051	1.6	0.072	1.790	1.995	0.264	3.815	3.815
0.0075	0.101	N/A	0	2.3	0.096	2.909	2.404	0.000	0.000	5.649
0.0075	0.101	N/A	0.071	1.9	0.096	2.718	1.905	0.000	0.000	1.270
0.0075	0.085	N/A		2.3	0.086	2.595	2.422	0.086	0.865	3.027
0.0075	0.085	N/A	0.071	1.9	0.086	2.233	2.037	0.140	1.395	3.209
0.0075	0.071	N/A	0	2.2	0.075	2.738	2.462	0.154	2.462	5.231
0.0075	0.071	N/A	0.051	1.9	0.075	2.030	1.970	0.182	1.970	2.424
0.0075	0.055	N/A	0	2.3	0.063	2.781	2.248	0.114	2.286	5.448
0.0075	0.055	N/A	0.031	2.0	0.063	2.277	2.195	0.207	3.727	5.383
0.0075	0.101	N/A	0	2.2	0.099	2.919	2.798	0.056	0.561	3.648
0.0005	0.055	N/A	0.051	1.5	0.074	2.216	1.946	0.081	1.465	4.315
0	0.101	N/A	0	1.5	0.175	1.697	1.691	0.160	0.800	1.200

Note: Both instantaneous and EA data analyses are included; Grayed data: EA data.

B.2. *Undular bore free-surface properties at $x = 8.5$ m (Present study)*

S_o	Q (m^3/s)	Radial gate opening (m)	h (m)	Fr_1	d_1 (m)	d_{max}/d_1	d_2/d_1	a_w/d_1	L_w/d_1
0	0.101	N/A	0.105	1.2	0.173	1.405	1.237	0.165	7.905
0	0.101	0.125	0.105	1.1	0.200	1.340	1.175	0.160	9.522
0	0.101	0.125	0.071	1.2	0.200	1.555	1.298	0.265	7.407
0	0.085	N/A	0.105	1.1	0.160	1.331	1.194	0.138	8.201
0	0.085	0.103	0.071	1.2	0.188	1.537	1.277	0.242	9.330
0	0.085	0.103	0.105	1.1	0.188	1.231	1.105	0.098	11.029
0	0.071	N/A	0.051	1.3	0.140	1.614	1.502	0.225	6.121
0	0.071	N/A	0.071	1.2	0.140	1.536	1.359	0.246	6.647
0	0.071	0.075	0.105	1.1	0.190	1.199	1.164	0.063	13.437
0	0.071	0.075	0.071	1.2	0.190	1.391	1.175	0.139	10.926
0	0.071	0.075	0.051	1.2	0.190	1.446	1.252	0.200	9.568
0	0.071	0.075	0.031	1.2	0.193	1.554	1.321	0.272	8.497

(*Continued*)

S_o	Q (m^3/s)	Radial gate opening (m)	h (m)	Fr_1	d_1 (m)	d_{max}/d_1	d_2/d_1	a_w/d_1	L_w/d_1
0	0.055	0.052	0.105	1.1	0.193	1.137	1.119	0.039	16.109
0	0.055	0.052	0.071	1.1	0.193	1.220	1.177	0.075	11.368
0	0.055	0.052	0.051	1.1	0.193	1.343	1.199	0.106	10.933
0	0.055	0.052	0.031	1.2	0.193	1.399	1.244	0.161	8.756
0	0.055	0.052	0.017	1.3	0.193	1.431	1.245	0.212	8.762
0	0.055	0.052	0	1.3	0.193	1.607	1.360	0.269	7.684
0	0.101	0.125	0.071	1.2	0.205	1.568	1.317	0.243	7.904
0	0.055	0.051	0.017	1.2	0.196	1.508	1.296	0.186	8.125

Note: Both instantaneous and EA data analyses are included; Grayed data: EA data.

References

Andersen, V. M. [1978] "Undular hydraulic jump," *J. Hydraul. Div.* **104**, 1185–1188. Discussion: **105**, 1208–1211.

Barré de Saint-Venant, A. J. C. [1871] "Théorie du Mouvement Non Permanent des Eaux, avec Application aux Crues des Rivières et à l'Introduction des Marées dans leur Lit," *C. R. Acad. Sci.* **73**(4), 147–154 (in French).

Bazin, H. [1865] "Recherches Expérimentales sur la Propagation des Ondes," *Mém. Acad. Sci.* **19**, 495–644 (in French).

Benjamin, T. B. & Lighthill, M. J. [1954] "On Cnoidal waves and bores," *Proc. R. Soc. Lond. A, Math. Phys. Sci.* **224**(1159), 448–460.

Benet, F. & Cunge, J. A. [1971] "Analysis of experiments on secondary undulations caused by surge waves in trapezoidal channels," *J. Hydraul. Res.* **9**(1), 11–33.

Boussinesq, J. V. [1871] "Théorie de l'Intumescence appelée Onde Solitaire ou de Translation se Propageant dans un Canal Rectangulaire," *C. R. Acad. Sci.* **72**, 755–759 (in French).

Boussinesq, J. V. [1877] "Essai sur la Théorie des Eaux Courantes," *Mém. Acad. Sci.* **23**(1), 1–680 (in French).

Bryson, A. E. [1969] "Film notes for waves in fluids," National Committee in Fluid Mechanics Films, No. 21611.

Chanson, H. [2005] "Physical modelling of the flow field in an undular tidal bore," *J. Hydraul. Res.* **43**(3), 234–244.

Chanson, H. [2010a] "Undular tidal bores: Basic theory and free-surface characteristics," *J. Hydraul. Eng.* **136**(11), 940–944, doi: 10.1061/(ASCE)HY.1943-7900.0000264.

Chanson, H. [2010b] "Unsteady turbulence in tidal bores: The effects of bed roughness," *J. Waterw. Port, Coast. Ocean Eng.* **136**.

Chanson, H. [2011a] *Tidal Bores, Aegir, Eagre, Mascaret, Pororoca: Theory and Observations* (World Scientific, Singapore), 220 pp.

Chanson, H. [2011b] "Turbulent shear stresses in hydraulic jumps and decelerating surges: An experimental study," *Earth Surf. Process. Landf.* **36**(2), 180–189, doi: 10.1002/esp.2031.

Chanson, H. [2012] "Momentum considerations in hydraulic jumps and bores," *J. Irrig. Drain. Eng.* **138**(4), 382–385, doi: 10.1061/(ASCE)IR.1943-4774.0000409.

Chanson, H. & Docherty, N. J. [2012] "Turbulent velocity measurements in open channel bores," *Euro. J. Mech. B/Fluids* **32**, 52–58, doi: 10.1016/j.euromechflu.2011.10.001.

Chanson, H., Reungoat, D., Simon, B. & Lubin, P. [2011] "High-frequency turbulence and suspended sediment concentration measurements in the Garonne river tidal bore," *Estuar. Coast. Shelf Sci.* **95**(2–3), 298–306, doi: 10.1016/j.ecss.2011.09.012.

Chanson, H. & Tan, K. K. [2010] "Turbulent mixing of particles under tidal bores: An experimental analysis," *J. Hydraul. Res.* **48**(5), 641–649, doi: 10.1080/00221686.2010.512779.

Chanson, H. & Toi, Y. H. [2015] "Physical modelling of breaking tidal bores: Comparison with prototype data," *J. Hydraul. Res.* **53**, 264–273, doi: 10.1080/00221686.2014.989458.

Chen, J., Liu, C., Zhang, C. & Walker, H. J. [1990] "Geomorphological development and sedimentation in Qiantang Estuary and Hangzhou Bay," *J. Coast. Res.* **6**(3), 559–572.

Docherty, N. J. & Chanson, H. [2012] "Physical modelling of unsteady turbulence in breaking tidal bores," *J. Hydraul. Eng.* **138**(5), 412–419, doi: 10.1061/(ASCE)HY.1943-7900.0000542.

Favre, H. [1935] Etude Théorique et Expérimentale des Ondes de Translation dans les Canaux Découverts, ('Theoretical and Experimental Study of Travelling Surges in Open Channels.') Dunod, Paris, France (in French).

Furgerot, L. [2014] *Propriétés hydrodynamiques du mascaret et de son influence sur la dynamique sédimentaire. Une approche couplée en canal et in situ* (*estuaire de la Sée*, *Baie du Mont Saint Michel*), ('*Hydrodynamic characteristics of a tidal bore and its impact on sediment dynamics. A combined laboratory and field study* (*Sée River estuary*, *Bay of Mount Saint Michel*).'), Ph.D. Thesis, University of Caen, laboratory M2C, France, 386 pp. (in French).

Furgerot, L., Mouaze, D., Tessier, B., Perez, L. & Haquin, S. [2013] Suspended sediment concentration in relation to the passage of a tidal bore (sée River Estuary, Mont Saint Michel, NW France), in *Proc. Coastal Dynamics 2013*, Arcachon, France, 24–28 June, pp. 671–682.

Furuyama, S. & Chanson, H. [2010] "A numerical solution of a tidal bore flow," *Coast. Eng. J.* **52**(3), 215–234, doi: 10.1142/S057856341000218X.

Gualtieri, C. & Chanson, H. [2011] "Experimental study of a positive surge. Part 2: Comparison with literature theories and unsteady flow field analysis," *Environ. Fluid Mech.* **11**(6), 641–651, doi: 10.1007/s10652-011-9222-3.

Gualtieri, C. & Chanson, H. [2012] "Experimental study of a positive surge. Part 1: Basic flow patterns and wave attenuation," *Environ. Fluid Mech.* **12**(2), 145–159, doi: 10.1007/s10652-011-9218-z.

Henderson, F. M. [1966] *Open Channel Flow* (MacMillan Company, New York, USA).

Hornung, H. G., Willert, C. & Turner, S. [1995] "The flow field downsteam of a hydraulic jump," *J. Fluid Mech.* **287**, 299–316.

Khezri, N. & Chanson, H. [2012] "Undular and breaking tidal bores on fixed and movable gravel beds," *J. Hydraul. Res.* **50**(4), 353–363, doi: 10.1080/00221686.2012.686200.

Koch, C. & Chanson, H. [2008] "Turbulent mixing beneath an undular bore front," *J. Coast. Res.* **24**(4), 999–1007, doi: 10.2112/06-0688.1.

Koch, C. & Chanson, H. [2009] "Turbulence measurements in positive surges and bores," *J. Hydraul. Res.* **47**(1), 29–40, doi: 10.3826/jhr.2009.2954.

Kucukali, S. & Chanson, H. [2008] "Turbulence measurements in hydraulic jumps with partially-developed inflow conditions," *Experi. Thermal Fluid Sci.* **33**(1), 41–53, doi: 10.1016/j.expthermflusci.2008.06.012.

Lemoine, R. [1948] "Sur les Ondes Positives de Translation dans les Canaux et sur le Ressaut Ondulé de Faible Amplitude," *Jl La Houille Blanche*, Mar–Apr., pp. 183–185 (in French).

Leng, X. & Chanson, H. [2015a] "Turbulent advances of a breaking bore: Preliminary physical experiments," *Experi. Thermal Fluid Sci.* **62**, 70–77, doi: 10.1016/j.expthermflusci.2014.12.002.

Leng, X. & Chanson, H. [2015b] "Breaking bore: Physical observations of roller characteristics," *Mech. Res. Commun.* **65**, 24–29, doi: 10.1016/j.mechrescom.2015.02.008.

Leng, X. & Chanson, H. [2015c] "Unsteady turbulence during the upstream propagation of undular and breaking tidal bores: An experimental investigation," Hydraulic Model Report No. CH98/15, School of Civil Engineering, The University of Queensland, Brisbane, Australia, 235 pp.

Lewis, A. W. [1972] *Field Studies of a Tidal Bore in the River Dee*, M.Sc. Thesis, Marine Science Laboratories, University College of North Wales, Bangor, UK.

Liggett, J. A. [1994] *Fluid Mechanics* (McGraw-Hill, New York, USA).

Lighthill, J. [1978] *Waves in Fluids* (Cambridge University Press, Cambridge, UK), 504 pp.

Lubin, P., Chanson, H. & Glockner, S. [2010] "Large eddy simulation of turbulence generated by a weak breaking tidal bore," *Environ. Fluid Mech.* **10**(5), 587–602, doi: 10.1007/s10652-009-9165-0.

Madsen, P. A., Simonsen, H. J. & Pan, C. H. [2005] "Numerical simulation of tidal bores and hydraulic jumps," *Coast. Eng.* **52**, 409–433, doi: 10.1016/j.coastaleng.2004.12.007.

Montes, J. S. [1986] "A study of the undular jump profile," in *Proc. 9th Australasian Fluid Mechanics Conf. AFMC*, Auckland, New Zealand, pp. 148-151.

Montes, J. S. [1998] *Hydraulics of Open Channel Flow* (ASCE Press, New-York, USA), 697 pages.

Murzyn, F., Mouaze, D. & Chaplin, J. R. [2007] "Air-water interface dynamic and free surface features in hydraulic jumps", *J. Hydraul. Res.* **45**(5), 679–685.

Murzyn, F. & Chanson, H. [2009] "Free-surface fluctuations in hydraulic jumps: Experimental observations," *Exp. Therm. Fluid. Sci.* **33**(7), 1055–1064, doi: 10.1016/j.expthermflusci.2009.06.003.

Pan, C. H., Ling, B. Y. & Mao, X. Z. [2007] "Case study: Numerical modeling of the tidal bore on the Qiantang River, China," *J. Hydraul. Eng.* **133**(2), 130–138.

Peregrine, D. H. [1966] "Calculations of the development of an undular bore," *J. Fluid Mech.* **25**, 321–330.

Rayleigh, L. [1908] "Note on tidal bores," *Proc. R. Soc. Lond. A*: *Math. Phys. Eng. Sci.* **81**(541), 448–449.

Reichstetter, M. [2011] *Hydraulic Modelling of Unsteady Open Channel Flow*: *Physical and Analytical Validation of Numerical Models of Positive and Negative Surges*, MPhil Thesis, School of Civil Engineering, The University of Queensland, Brisbane, Australia, 112 pp.

Reungoat, D., Chanson, H. & Caplain, B. [2014] "Sediment processes and flow reversal in the undular tidal bore of the Garonne river (France)," *Environ. Fluid Mech.* **14**(3), 591–616, doi: 10.1007/s10652-013-9319-y.

Reungoat, D., Chanson, H. & Keevil, C. E. [2015] "Field measurements of unsteady turbulence in a tidal bore: The Garonne river in October 2013," *J. Hydraul. Res.* **53**(3), 291–301, doi: 10.1080/00221686.2015.1021717.

Richard, G. L. & Gavrilyuk, S. L. [2013] "The classical hydraulic jump in a model of shear shallow-water flows," *J. Fluid Mech.* **725**, 492–521.

Shuto, N. [1985] "The Nihonkai–Chubu earthquake tsunami on the North Akita coast," *Coastal Eng. Japan* **20**, 250–264.

Simon, B. & Chanson, H. [2013] "Turbulence measurements in tidal bore-like positive surges over a rough bed," Hydraulic Model Report No. CH90/12, School of Civil Engineering, The University of Queensland, Brisbane, Australia, 176 pp.

Spiegel, M. R. [1972] *Theory and Problems of Statistics* (McGraw-Hill, New York, USA).

Sun, S., Leng, X. & Chanson, H. [2016] "Rapid operation of a tainter gate: Generation process and initial upstream surge motion," *Environ. Fluid Mech.* **16**(1), 87–100, doi: 10.1007/s10652-015-9414-3.

Tanaka, H., Tinh, N. X. & Dao, N. X. [2011] "Field measurement and numerical studies on the tsunami propagation into upstream rivers," in *Proc. 34th IAHR World Congr.*, Brisbane, Australia, 26 June–1 July, eds. Valentine, E. M., Apelt, C. J., Ball, J., Chanson, H., Cox, R., Ettema, R., Kuczera, G., Lambert, M., Melville, B. & Sargison, J., pp. 1317–1324.

Tanaka, N., Yagisawa, J. & Yasuda, S. [2012] "Characteristics of damage due to tsunami propagation in river channels and overflow of their embankments in great East Japan earthquake," *Int. J. River Basin Manag.* **10**(3), 269–279.

Tolkova, E., Tanaka, H. & Roh, M. [2015] "Tsunami observations in rivers from a perspective of tsunami interaction with tide and riverine flow," *Pure Appl. Geophys.* **172**, 953–968, doi: 10.1007/s00024-014-1017-2.

Treske, A. [1994] "Undular bores (favre-waves) in open channels — Experimental studies," *J. Hydraul. Res.* **32**(3), 355–370. Discussion: **33**(3), 274–278.

Tricker, R. A. R. [1965] *Bores*, *Breakers*, *Waves and Wakes* (American Elsevier, New York, USA).

Valiani, A. [1997] "Linear and angular momentum conservation in hydraulic jump," *J. Hydraul. Res.* **35**(3), 323–354.

Wang, H. & Chanson, H. [2015] "An experimental study of turbulent fluctuations in hydraulic jumps," *J. Hydraul. Eng.* **141**, 10 pp., doi: 10.1061/(ASCE)HY.1943-7900.0001010.

Wang, H., Murzyn, F. & Chanson, H. [2014] "Total pressure fluctuations and two-phase flow turbulence in hydraulic jumps," *Experi. Fluids* **55**(11), 16 pp., doi: 10.1007/s00348-014-1847-9.

Wolanski, E., Williams, D., Spagnol, S. & Chanson, H. [2004] "Undular tidal bore dynamics in the daly estuary, Northern Australia," *Estuar. Coast. Shelf Sci.* **60**(4), 629–636, doi: 10.1016/j.ecss.2004.03.001.

Yeh, H. H. & Mok, K. M. [1990] "On turbulence in bores," *Phys. Fluids A* **A2**(5), 821–828.